Areal Density Measurement of Laser Targets Using Absorption Lines

Absorption lines due to 1*s*–2*p* transitions in titanium ions are predicted to be observed in the implosion of titanium-doped shells. The measured absorption of these lines can be used to determine the peak areal density $\rho\Delta r$ of the doped layer and hence of the total compressed shell. The absorption lines are studied by solving the radiation transport equation using opacity tables and hydrodynamic simulations. The absorption is a function not only of $\rho\Delta r$ but also of the density and temperature of the absorbing layer. However, it is shown that the areal density can be estimated with reasonable accuracy by using the measured intensity of absorption and its distribution over the various absorption lines. The considerations affecting the choice of doping parameters are discussed, as well as the effect of integrating the measured spectrum over time and target volume.

Recently published work[1] showed that a titanium-doped layer within a polymer shell of a laser-imploded target can yield information on core-shell mixing. We show here that the absorption lines predicted to be produced by such a doping provide a signature of shell areal density ($\rho\Delta r$) at peak compression. This areal density is an important parameter characterizing the implosion performance, which in turn is determined by target instability and mixing.

In the work on mixing diagnostics,[1] the doped-layer location within the shell was removed from the fuel-shell interface so that, in the absence of mixing, only titanium absorption lines would be observed, but mixing could cause titanium material to move into inner target regions and emit titanium lines. Even for the assumed level of mixing, *the absorption lines were essentially unchanged from the no-mixing case*. Thus, such a doped layer can provide information on the overall $\rho\Delta r$ of the compressed (or overdense) shell, even if its inner part undergoes mixing. The doped layer is placed in the target far from the interface but still close enough not to be ablated away.

Measurement of the absorption spectrum yields the areal density of only the doped layer.[2] This by itself is of interest because the comparison of measured and predicted $\rho\Delta r$ for the doped layer is a measure of target performance. Additionally, the total areal density of the compressed shell can be deduced if the thickness of target layer that is ablated away is measured (e.g., by charge collectors).

The absorption lines are studied by solving the radiation transport equation using OPLIB[3] opacity tables and one-dimensional *LILAC*[4] hydrodynamic simulations. The absorption is a function not only of $\rho\Delta r$ but also of the density and temperature of the absorbing layer. However, it is shown that the areal density can be estimated with reasonable accuracy by using the measured intensity of absorption and its distribution over the various absorption lines. The initial $\rho\Delta r$ of the titanium doping must be small enough, or the effect of local emission in the absorption region will lead to underestimating the $\rho\Delta r$. It is further shown that integrating the measured spectrum over the target volume causes only a small error, while integrating over time causes the $\rho\Delta r$ to be underestimated by about a factor of 2.

Modeling a Test Case

We calculate the expected x-ray spectrum of a particular simulated target implosion on the OMEGA laser. For this test case, *LILAC* results were used for the expected temperature (T) and density (ρ) profiles, and a post-processor[5] code was used to calculate the emission and radiation transport through the target. To simulate the emergent absorption and emission spectrum, multigroup opacity tables were generated using the OPLIB opacity library.[3]

The target is a polymer shell of 940-μm diam and 30-μm thickness, filled with 80 atm DT gas. A layer doped with 1% titanium (by atom number) is embedded in a CH polymer shell; the doped layer is placed 2.4 μm from the interface and its thickness is varied. As explained in earlier work,[1] such a doped layer shows significant absorption at the wavelengths of titanium lines, while showing little effect on overall target behavior. The laser pulse is trapezoidal, rising linearly over a 0.1-ns period to 13.5 TW, then remaining constant for 2.2 ns, before dropping linearly over a 0.1-ns period. *LILAC* hydrody-

namic simulations show[1] that the shell compresses to a mean radius of ~50 μm and thickness of ~30 μm, with a density in the range of ~10 to 50 g/cm^3, corresponding to a $\rho\Delta r$ value of ~90 mg/cm^2. The electron temperature in the shell ranges from ~800 (at the shell-fuel interface) to ~80 eV (at the peak of the shell density); the line absorption occurs within the colder, outer part of this compressed shell. The profiles at maximum compression are shown in Fig. 69.11.

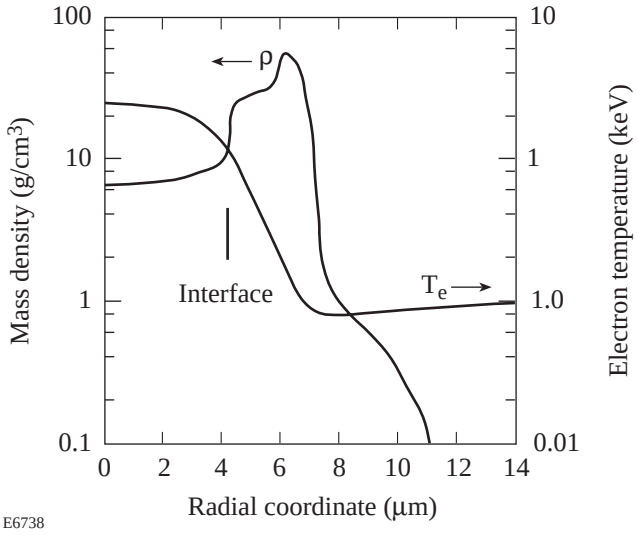

Figure 69.11
The density and temperature profiles predicted by the *LILAC* hydrodynamics simulation code at peak compression.

Figure 69.12 shows examples of the predicted spectrum at two instances during the implosion, showing titanium absorption lines. The time 2.9 ns corresponds to peak compression. These lines correspond to transitions of the type 1*s*–2*p* in titanium ions of an incomplete *L* shell: Ti^{+13} to Ti^{+20}. The designation Li in Fig. 69.12 stands for lithium-like titanium ion, and likewise for the other designations. Each peak contains several lines that are unresolved mostly because of broadening due to the finite source size. For example, the peak marked *C* (carbon-like) consists of 35 transitions of the type $1s^2 2s^2 2p^2$–$1s 2s^2 2p^3$. On approaching peak compression, the intensity of the continuum radiation is seen to rise sharply and the absorption-line manifold is seen to shift to higher ionization states. This shift, caused by the increase in shell temperature as the shell becomes more compressed, is discussed further below.

The absorption lines are formed when radiation emitted by the compressed core traverses colder shell layers. By the definition of the opacity *k*, the intensity within an absorption

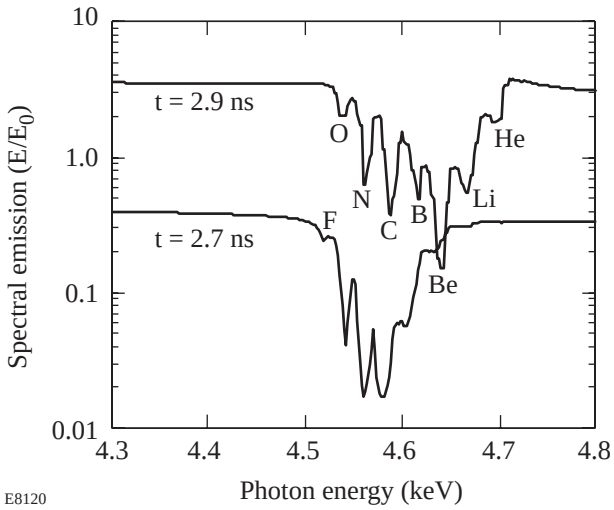

Figure 69.12
The predicted spectrum emitted by the test case (1%-titanium-doped layer) at two times during the implosion; $E_0 = 7 \times 10^{15}$ keV/(keV ns Ω). The time 2.9 ns corresponds to peak compression. The designation Li stands for the lithium-like titanium ion, and likewise for the other designations. The emission is integrated over the target volume.

line at an energy *E* is given by

$$I(E) = I_0(E)\,\exp\left[-\int k(E)\rho dr\right], \qquad (1)$$

where I_0 is the core-emitted intensity and $k(E)$ is the opacity per unit areal density. Equation (1) assumes that the local emission within the absorption region is neglected; this point is discussed further below. From Eq. (1) it follows that the $\rho\Delta r$ of the absorbing layer can be deduced from the measured spectrum through the relationship $\rho\Delta r = \ln\left[I_0(E)/I(E)\right]/k(E)$. However, $k(E)$ depends also on the (unknown) temperature and density in the absorption layer. Note that the density dependence of the opacity is in addition to the explicit dependence of the attenuation on $\rho\Delta r$ [Eq. (1)]. Next we examine these dependencies and show how Eq. (1) can be used to estimate the $\rho\Delta r$ of the absorbing layer, even without an exact knowledge of the temperature and the density.

Areal Density Determination Using Absorption Lines

Figures 69.13 and 69.14 show examples from OPLIB[3] of the opacity spectrum for 1% titanium in CH, as a function of temperature and density. As seen, 1%-titanium doping provides an ample contrast ratio between line absorption by titanium ions and the nonresonant absorption by both titanium

and CH. As the temperature increases (Fig. 69.13), the absorption-line manifold shifts to higher photon energies, or higher ionizations. The shift seen in Fig. 69.12 is similarly due to an increase in shell temperature on approaching peak compression. On the other hand, Fig. 69.14 shows that for the same temperature, a higher density causes the manifold to shift to lower ionizations. This is because the three-body (or collisional) recombination increases with increasing density faster than the two-body collision processes. The three-body recombination is important only at or near LTE (local thermodynamic equilibrium),[6] which is the atomic model used to generate the OPLIB tables. However, it can be shown[7] that for the ions and temperatures under consideration, the LTE approximation for the distribution of ion populations holds for densities (of the mostly polymer material) higher than ~6 g/cm^3; much higher shell densities than this are predicted for the test case. From Fig. 69.13 a doubling of the temperature leads to a 0.05-keV shift in the peak absorption. A similar shift in peak absorption requires, from Fig. 69.14, a factor-of-10 increase in density. Thus the peak positions are more sensitive to changes in temperature than in density. Figures 69.13 and 69.14 clearly show that the absorption at any given photon energy depends on both the temperature and the density; consequently, Eq. (1) cannot be used in a simple way to derive $\rho\Delta r$. In addition it should be noted that (1) changes in temperature and density cause primarily an energy shift in the absorption lines and (2) the total absorption-line manifold has only a weak dependence on temperature and density. Thus we choose the integral $\int \ln[I_0(E)/I(E)]\,dE$ over the whole absorption-line manifold as the experimental signature. We refer to the integral $\int \ln(I_0/I)\,dE$ as the area within the absorption lines [if film density is proportional to ln(I), this indeed is the area under the absorption lines on film]. From Eq. (1) we obtain

$$\int \ln[I_0(E)/I(E)]\,dE = \rho\Delta r \int k(E)\,dE\,. \qquad (2)$$

The opacity integral on the right can be obtained from opacity spectra such as those in Figs. 69.13 and 69.14. It turns out that even after integrating the opacity over the absorption-line manifold, the opacity still depends appreciably on temperature and density. For example, the opacity varies from 35 to 85 cm^2 keV/g when the temperature is varied from 0.3 to 10 keV and the density is varied from 1 to 50 g/cm^3. However, in addition to the integral over the spectrum we can also make use of the measured distribution among the absorption peaks. More specifically, the peak of strongest absorption provides an additional signature that also depends on both temperature and density and helps to narrow the range of opacity values.

To make use of this additional information, we calculated the integrated opacity for temperatures in the range of 0.3 to 1.0 keV and densities in the range of 1 to 50 g/cm^3. Fig-

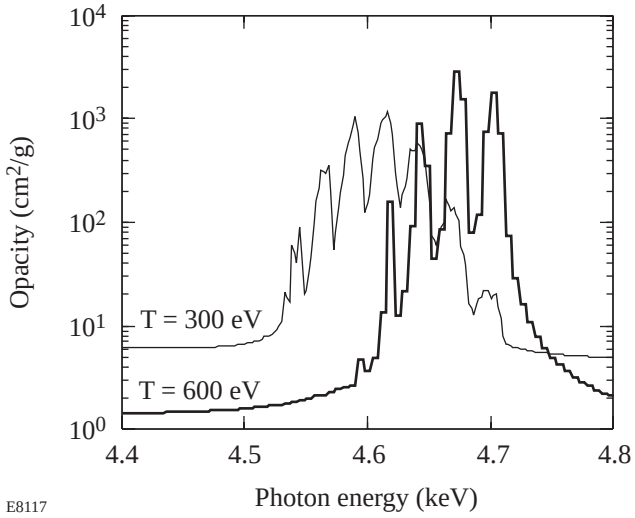

Figure 69.13
The opacity of 1%-titanium-doped CH at a density of 3.2 g/cm^3 (from OPLIB[3]), showing a shift to higher photon energies (higher ionizations) with increasing temperature. The absorption lines are due to 1*s*–2*p* transitions in titanium ions with increasing number of *L*-shell vacancies.

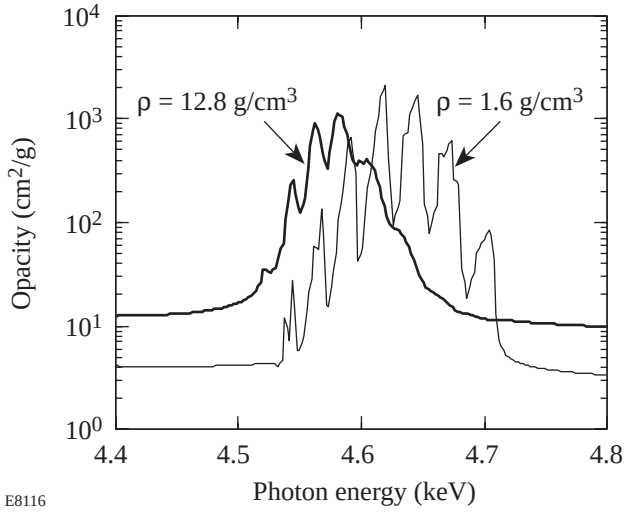

Figure 69.14
The opacity of 1%-titanium-doped CH at a temperature of 300 eV, showing a shift to lower photon energies (lower ionizations) with increasing density.

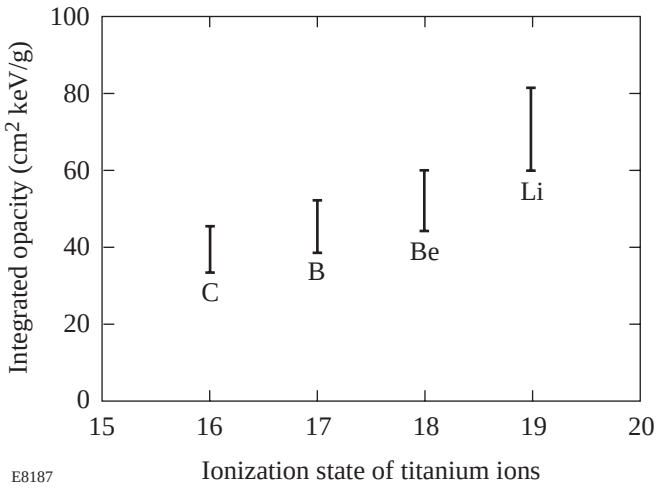

Figure 69.15
Area under the opacity-spectrum peaks, such as those in Figs. 69.13 and 69.14. For temperatures in the range of 300 to 1000 eV and densities in the range of 1 to 50 g/cm^3, the points are grouped according to the strongest absorption peak in the opacity spectrum (Li stands for cases where the lithium-like peak is the strongest, and likewise for the other designations).

ure 69.15 shows the results, arranged according to the strongest opacity peak (marked Li for cases where the lithium-like peak is the strongest, etc.). The four charge states (C-like to Li-like) cover the range likely to be encountered in target implosions. Figure 69.15 shows that knowing the peak of maximum absorption (without knowing the temperature or the density) narrows down the range of integrated opacity from ±42% to within ±15%.

To apply Fig. 69.15 to an experimental result, we first note the peak of maximum absorption in the spectrum. For example, if the Be-like peak dominates, we obtain from Fig. 69.15 the value 52 for the integrated opacity $\int k(E)dE$, *without having to know the temperature or the density*. Substituting this value in Eq. (2) produces a relation between the $\rho\Delta r$ of the doped layer and the measured area within the absorption lines (the integral on the left side of the equation). The error in determining $\rho\Delta r$ based of Fig. 69.15 is ±15%; other sources of error are discussed below.

Using the area under the absorption lines rather than the intensity profiles obviates the need to know the line profiles (e.g., due to Doppler and Stark effects). However, the measured and calculated intensity profiles should actually be quite similar because the absorption profile for each ion specie is comprised of many closely spaced components. In the experiment these components are smeared by the source-size broadening, whereas in the OPLIB[3] calculations they are smeared by the energy bin width, chosen to be similar to the source-size broadening. The final absorption profile for each ion specie is the envelope over these components and depends mostly on their relative intensity and separation.

Application of the Method to a Simulated Implosion

To test the method of determining $\rho\Delta r$ by the spectrum of absorption lines we apply it to a simulated spectrum from the implosion of the test case and compare the resulting $\rho\Delta r$ to the actual $\rho\Delta r$ of the profiles used in the calculation of the spectrum. This procedure simulates the application of the method to an experimentally observed spectrum.

Figure 69.16 shows two examples of the calculated emergent spectrum for the test case. For very high opacities, the attenuation in the emergent lines cannot be arbitrarily high because local emission within the absorption region fills in the absorption dips. Therefore, the doped layer must be sufficiently thin, or the $\rho\Delta r$ will be underestimated. Similarly, the depth of the observed absorption lines is limited by the finite dynamic range of the film (or other detector). To demonstrate the effect of self-absorption, we show in Fig. 69.16 a comparison of the spectra emitted from two identical titanium-doped targets except for the thickness of the doped layer, which was

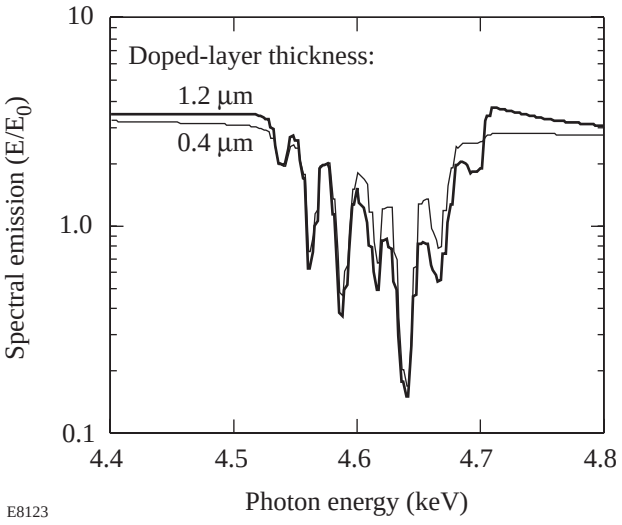

Figure 69.16
Comparison of the spectrum emitted from two identical 1%-titanium-doped targets except for the thickness of the doped layer, which was 0.4 and 1.2 μm, respectively. Both spectra refer to the time of peak compression and are integrated over the target volume; $E_0 = 7 \times 10^{15}$ keV/(keV ns Ω). The near coincidence of the two spectra is caused by the local emission in the absorption region.

0.4 and 1.2 μm, respectively. We refer to these two target simulations as the "thin case" and the "thick case." The separation of the outer surface of the doped layer from the shell-fill interface was 2.4 μm in both cases (the thick case's inner boundary was closer to the shell-fill interface than the thin case's). Both spectra refer to the time of peak compression and are integrated over the target volume. The similarity of the two spectra is clear evidence of local emission in the absorption region. Thus, at the wavelengths of highest absorption, only radiation emitted on the outer surface of the doped layer can emerge, and its intensity is independent of the thickness of the doped layer. On the other hand, for the weak absorption peaks [where the attenuation factor $\ln(I_0/I)$ is smaller than ~1] we would expect the absorption depths to be proportional to the doped-layer thickness. The reason for the weaker changes evident in Fig. 69.16 is that the thin doped layer happens to sample the highest-absorbing part (higher ρ, lower T) of the doped region. Thus, a too-thick doped layer gives rise to difficulties due to both local emission and gradients in plasma parameters.

We now apply the method of determining the areal density to the two spectra in Fig. 69.16. The area $\int \ln(I_0/I)\,dE$ in Fig. 69.16 is equal to 0.17 keV for the thin case and 0.21 keV for the thick case. The strongest absorption peak is at 4.65 keV and corresponds to Be-like titanium. From Fig. 69.15 we use the average integrated opacity for the Be-like titanium, which has the value 52 cm^2 keV/g (with an error of ±15%). Substituting these values into Eq. (2) we finally obtain $\rho\Delta r$ = 3.2 mg/cm^2 for the thin case and $\rho\Delta r$ = 4.0 mg/cm^2 for the thick case. This is compared with *LILAC*'s $\rho\Delta r$ values at peak compression: $\rho\Delta r$ = 3.1 mg/cm^2 for the thin case and $\rho\Delta r$ = 13.5 mg/cm^2 for the thick case. Thus, the method works well for the thin case but significantly underestimates the $\rho\Delta r$ in the thick case because of local emission within the absorption region.

To obtain accurate $\rho\Delta R$ measurements from this technique the target doping must be such that $k\rho\Delta r < 1$, which can be achieved in two ways: The choice of target doping can be based on simulations, or one can start with high-$\rho\Delta r$ doping and repeat the experiment with successively lower doping levels until the measured absorption is seen to decrease with decreasing doping. The latter procedure is also desirable for the following reason: if the achieved $\rho\Delta r$ is smaller than predicted, the absorption lines may not be observed at all. Thus, starting with a thicker doped layer ensures the observation of absorption lines even in such a case. In the test case studied here, a 0.4-μm-thick layer doped at 1% was shown to be an appropriate final choice for doping.

The emergent spectrum from the simulated target has been shown in earlier publications.[1] However, that spectrum was computed for a spatially and temporally resolved measurement (axial view at peak compression). We show here the effect of integrating the calculated emergent spectrum over space and time. First, Fig. 69.17 shows a comparison of an axial-view spectrum (per unit area) with the space-integrated spectrum. The spectral intensity refers to the flux per unit area in units of $I_0 = 7\times10^{20}$ keV/(keV ns cm^2 Ω), whereas the emission refers to the flux from the whole target in units of $E_0 = 7\times10^{15}$ keV/(keV ns Ω). The ratio between the two curves is essentially equal to the inverse of the cross section of the emitting core (giving in Fig. 69.17 a core diameter of ~80 μm). The two spectra have very similar shapes, and the spatially integrated spectrum has an area $\int \ln(I_0/I)\,dE$ that is only ~15% smaller than that of the spatially resolved spectrum. This is not surprising since any ray from the core in the direction of observation traverses essentially the same shell thickness.

Figure 69.18 shows a comparison between the emergent spectrum at the time of peak compression (2.9 ns) and the time-integrated spectrum; both are integrated over the target volume. Note that the peak in absorption for the time-integrated spectra is not as clear cut as the peak for the time-resolved spectra. As

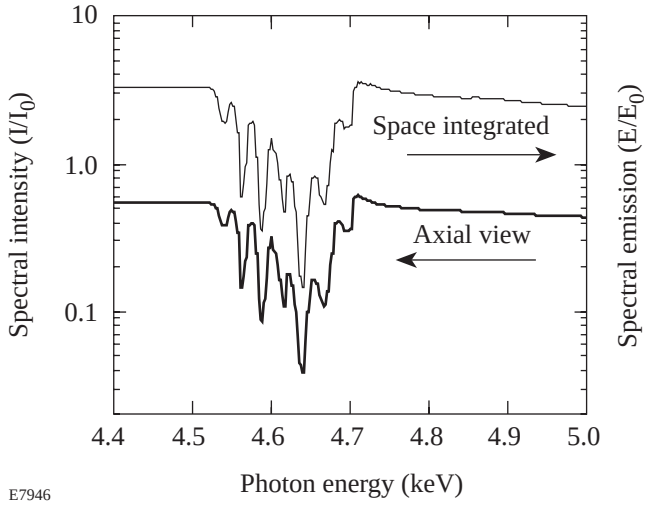

Figure 69.17
Comparison of simulated axial-view spectrum (per unit area) and space-integrated spectrum from an imploded, 1%-titanium-doped target. $I_0 = 7\times10^{20}$ keV/(keV ns cm^2 Ω); $E_0 = 7\times10^{15}$ keV/(keV ns Ω). The ratio between the two is essentially equal to the inverse of the cross section of the emitting core.

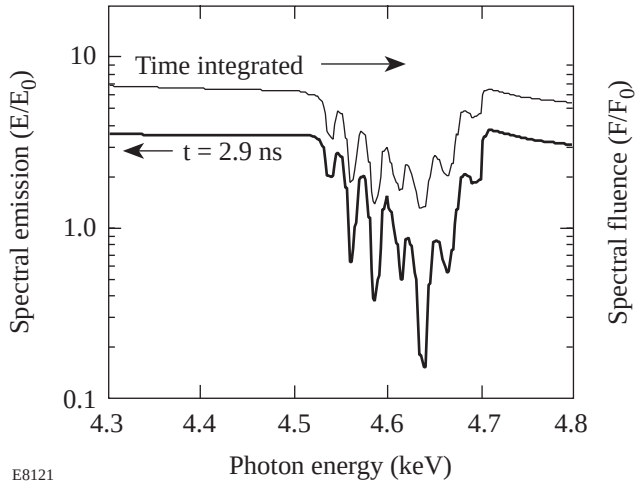

Figure 69.18
Comparison of simulated peak-compression and time-integrated spectra from an imploded, 1%-titanium-doped target (both are integrated over the target volume). $E_0 = 7 \times 10^{15}$ keV/(keV ns Ω); $F_0 = 2.3 \times 10^{15}$ keV/(keV Ω). The ratio between the two curves is essentially equal to the inverse of the core emission duration in nanoseconds.

the implosion progresses, the titanium dopant experiences an increase in temperature and density, and consequently there is a shift in the absorption peak with time. The time-integrated measurement averages over all these peaks. The emission, as in Fig. 69.17, is in units of $E_0 = 7 \times 10^{15}$ keV/(keV ns Ω) and the fluence is in units of $F_0 = 2.3 \times 10^{15}$ keV/(keV Ω). The ratio between the two curves is essentially equal to the inverse of the core emission duration in nanoseconds (Fig. 69.18 gives a duration of ~0.6 ns). The area $\int \ln(I_0/I)\,dE$ for the time-integrated spectrum is about half that of the peak-emission spectrum and using it would result in an underestimate of the $\rho\Delta r$ by the same factor.

As mentioned earlier, the total $\rho\Delta r$ of the compressed shell, $(\rho\Delta r)_{\text{total}}$, can be deduced from that of the doped layer, $(\rho\Delta r)_{\text{doped}}$, if the total ablated mass is measured (e.g., by charge collectors). A simple geometrical consideration shows that for a *uniformly compressed shell* the ratio

$$(\rho\Delta r)_{\text{doped}} / (\rho\Delta r)_{\text{total}}$$

is proportional to its initial value through a proportionality constant C, which depends on the spherical convergence and the location of the doped layer within the shell; C is smaller than, but close to 1. In the simulated test case the density of the compressed shell was constant to within ±30%. For that case, with an initial 30-μm-thick shell and a 0.4-μm-thick doped layer (the thin case), we deduced above a $\rho\Delta r$ for the doped layer of 3.2 mg/cm^2. The simulations by *LILAC* show that 16 μm of the shell thickness is unablated (this in an experiment will be deduced from charge collectors), so the total shell areal density at peak compression is estimated as $\rho\Delta r = 3.2 \times (16/0.4) = 128$ mg/cm^2. Here we assumed that the convergence is unknown and used $C = 1$. This result compares with *LILAC*'s value for peak compression of $\rho\Delta r = 110$ mg/cm^2. If the convergence is known (for example, from imaging), a better value of C can be used and the discrepancy reduced.

It might be thought that a thicker layer doped at a lower concentration could reduce the problem of relating the measured $\rho\Delta r$ to that of the total shell. However, this is undesirable because enlarging the doped layer results in averaging over the steep temperature gradient in the shell. This introduces an uncertainty in the choice of peak to be used in Fig. 69.15 and thus an additional error in the derived areal density.

Conclusion

An effective method has been described for measuring the areal density of the compressed (or overdense) shell of laser-imploded targets, based on the observation of absorption lines from a titanium-doped layer. Four factors have been shown to affect the precision of such measurement:

(a) If the initial $\rho\Delta r$ of the doped layer is too high, the problem of local emission in the absorption region will lead to an underestimate of the $\rho\Delta r$ at peak compression. To address this problem, the experiment can be repeated with progressively thinner doped layers (or lower doping concentrations), until the absorption is seen to decrease with decreasing $\rho\Delta r$ of the initial doped layer. This procedure is also desirable to ensure the observation of absorption lines even if the actual compression is smaller than predicted.

(b) If the spectrum is not streaked in time, the $\rho\Delta r$ will be grossly underestimated (typically by a factor of 2).

(c) If the spectrum is not spatially resolved, the $\rho\Delta r$ will be slightly underestimated (typically by ~15%). Thus, it is more important to resolve the spectrum in time than in space.

(d) The total ablated mass must first be determined (for example, by employing charge collectors) to be able to relate the measured $\rho\Delta r$ of the doped layer to the total $\rho\Delta r$ of the overdense shell.

ACKNOWLEDGMENT

This work was supported by the U.S. Department of Energy Office of Inertial Confinement Fusion under Cooperative Agreement No. DE-FC03-92SF19460, the University of Rochester, and the New York State Energy Research and Development Authority. The support of DOE does not constitute an endorsement by DOE of the views expressed in this article.

REFERENCES

1. B. Yaakobi, R. S. Craxton, R. Epstein, and Q. Su, J. Quant. Spectrosc. Radiat. Transfer **55**, 731 (1996).

2. A. Hauer, R. D. Cowan, B. Yaakobi, O. Barnouin, and R. Epstein, Phys. Rev. A **34**, 411 (1986).

3. M. F. Argo and W. F. Huebner, J. Quant. Spectrosc. Radiat. Transfer **16**, 1091 (1976).

4. E. Goldman, Laboratory for Laser Energetics Report No. 16, 1973 (unpublished); J. Delettrez and E. B. Goldman, Laboratory for Laser Energetics Report No. 36, 1976 (unpublished).

5. Laboratory for Laser Energetics LLE Review **58**, NTIS document No. DOE/SF/19460-17, 1994 (unpublished), p. 57.

6. H. R. Griem, *Plasma Spectroscopy* (McGraw-Hill, New York, 1964), Chap. 6.

7. *ibid.*, Eq. (6-60).